Contents

Abstract

An ensemble of camphor particles floating on water may exhibit a variety of collective behaviors. Some of these closely resemble group behaviors seen in more common systems such as ant colonies and vehicle traffic, so it is useful to study camphor particles as a model of collective dynamics. Several different types of camphor particles on various water surface configurations have been studied experimentally. In this work, a few common setups are investigated through numerical simulation and analysis of mathematical models. The results closely resemble experimental observations, and most of the observed patterns are reproduced and analyzed. Some additional behaviors are also observed that are awaiting experimental verification. There remain some challenges and open questions that will be the subject of future study.

1 Introduction

1.1 Collective motion in nature

Throughout numerous fields of science and engineering, research is done on collections of similar entities that influence each other in some way, quite often in a way that affects their movement. Imagine, for example, a school of fish flowing in beautiful coordination, or the aggravating congestion of cars on a busy highway. Such topics of study are examples of collective motion, a broad subcategory of collective behavior. The interactions between entities could be as simple as physical collisions between inanimate objects, or as complex as leadership selection among a flock of flying birds. Biology presents an especially rich variety of such systems because most of the countless varieties of animals are mobile and must interact with other members of their species. A few nonliving collections of driven, inanimate objects have also been studied [1, 2, 3, 4, 5, 6].

Despite the immense diversity, recent efforts have shown progress in unifying similar types of collective motion into universality classes. In this way, it is possible to understand a broad class of collective dynamics by studying relatively simple model systems. The camphor particles investigated in this work are an example of the class of self propelled particles, introduced by Vicsek [7]. As the name implies, these objects propel themselves independently and their motion is influenced by other nearby objects in the group. The original rule-based definition of self propelled particles is mathematically interesting and can display a variety of complex behaviors including kinetic phase transitions [7, 8, 9, 10] and large scale pattern formation [11], but it does not directly correspond to any physical system. Several modified versions have also been made to model more physically realistic objects [12, 13, 14, 15]. Here I will use the term loosely to encompass a more diverse array of systems including groups of fish, insects, humans, some inanimate objects, etc.

1.2 Camphor as a model system

The self induced motion of camphor on water has been studied for over a century. One of the first explanations for this behavior is attributed to Van der Mensbrugghe, who realized that it was due to a change in surface tension. More recent experimental work has focused on characterizing the various dynamical patterns that depend on particle shape and size [16, 17], water surface geometry [1, 18, 19, 20, 21], and additional chemical influences [19, 22, 23, 24, 25]. Some work has also been done concerning the collective behavior of groups of camphor particles including powder [26], solid pellets [27], and boats containing some plastic structure [1, 4, 5, 6, 28, 29]. The investigation presented here is based on camphor boats, which are described in more detail in the next section.

Along with many of these experimental results, theoretical models and simulations have been used to better understand the key features of the motion. Such models are typically based on the driving force of surface tension gradients acting against the damping effect of viscosity. Since many interesting dynamical patterns can be reproduced with the models, it seems that these two influences are sufficient to approximate the behavior of camphor particles on water.

The simplicity of the theoretical model and the relative ease of experimentation make this attractive as a model system for collective motion. An ensemble of these particles interacts primarily through their influence on the camphor distribution on the water surface. This indirect interaction through a background field has some similarity to a colony of ants communicating through pheromone trails, or to bacteria sensing chemical gradients. As described in section 3.2, camphor boats do indeed display some collective phenomena very similar to the motion of ants. It is hoped that further investigation will reveal more similarities between the collective dynamics of camphor particles and the countless examples seen in nature.

2 Model and simulation method

2.1 Setup

The term camphor boat has been used to describe a variety of different buoyant structures containing a camphor source. To avoid confusion, it will be used throughout this work to describe the three specific configurations detailed below. Any other camphor object will be described explicitly when needed. The basic construction of a camphor boat consists of an inert, buoyant disk located at the air water interface. As it corresponds to the plastic disk used in experiment, it will be labeled as such. Attached to the underside of the plastic is a disk of camphor. The diameter of the camphor may be the same as or smaller than that of the plastic. When the two disks are aligned concentrically, the structure is labeled a symmetric boat. When the centers are offset, it is labeled an asymmetric boat. Unless otherwise stated, asymmetric boats will have the center of the camphor disk placed at the edge of the plastic disk. Diagrams of these different configurations are shown in figure 1.

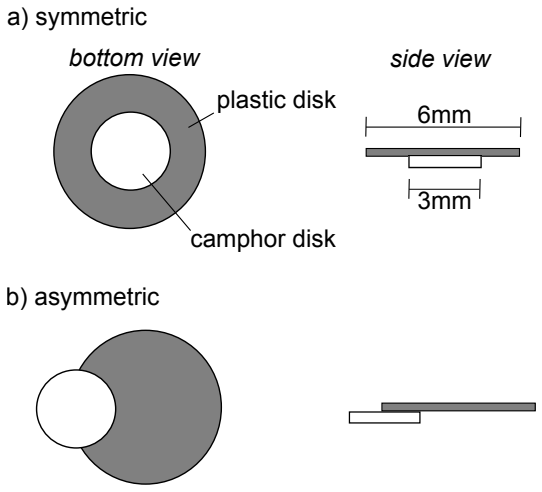

Figure 1: A schematic drawing of (a)symmetric and (b)asymmetric boats. A symmetric boat with equal plastic and camphor diameters is used to model the camphor pellets used in some experiments.

Boats of this type are placed in narrow channels that restrict movement to essen-

tially one dimension. This has the advantage of greatly simplifying analysis of their motion. Linear channels give the best approximation to a truly one dimensional system, but are practically limited in length. To eliminate end barriers, periodic routes with various geometries have also been used [1, 28]. Circular channels, such as the one shown in figure 2, can be constructed specifically for this purpose, but recent experiments have made use of two petri dishes of different diameter, one placed inside the other. The channels used in experiment introduce effects that are not accounted for in the model. For example, the meniscus creates an uneven topology that may affect the motion of boats. Also, in some cases significant sideways motion and collisions with the walls can be seen.

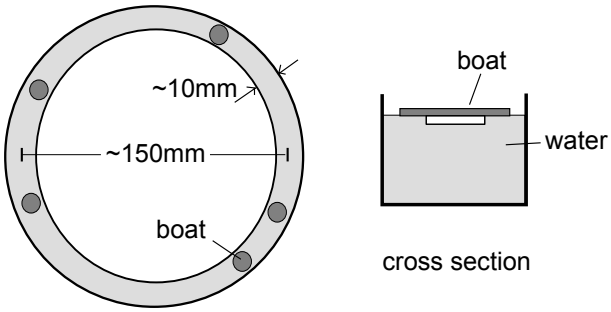

Figure 2: Schematic drawing of a one-dimensional periodic route. Not to scale.

In simulation, true one-dimensional periodic routes are used. Boats are described by line segments with surface tension acting on the two ends. Of course, surface tension and viscous forces must be computed for a boat with finite width. Two-dimensional simulations were also carried out including such effects as wall collisions and the circular shape of the boats.

2.2 Basic equations

The basic model consists of two differential equations. The first, equation 1, describes the dynamics of each boat. Define the position of boat number i, where $i = 1, 2, ...N$, as $\mathbf{x_i}$. m is the mass of the boat. Then the first term on the right side of the equation is a linear viscous resistance with viscosity constant μ. The second term is the net surface tension integrated around the edge of the boat. It acts perpendicular to the edge along normal vector $\mathbf{n}$. In the one-dimensional case, this integral is simply the difference between the two sides of the boat. The surface tension, $\gamma(c)$, depends on the surface camphor density, c, according to equation 2. γ_{water} and $\gamma_{camphor}$ are the surface tension of pure water and camphor saturated solution respectively. This relation was chosen to qualitatively match experimental observations. Other functions have been used in the past [4, 18, 20, 28], and the sigmoidal shape is a key feature. β is a normalizing parameter that sets the scale of the relation.

$$\frac{\partial^2 \mathbf{x}_i}{\partial t^2} = -\frac{\mu}{m}\frac{\partial \mathbf{x}_i}{\partial t} + \frac{1}{m}\int_{edge} \gamma(c)\mathbf{n}ds \tag{1}$$

$$\gamma(c) = \frac{\gamma_{water} - \gamma_{camphor}}{(\beta c)^2 + 1} + \gamma_{camphor} \tag{2}$$

For the case of one dimension, these equations can be combined and more easily written by defining the boat's position as the center of the plastic disk as in equation 3. Note the factor of L in the last term meaning that the surface tension is acting

on an edge with length L on either side of the boat. This more closely corresponds to a plastic square, but it is a simplifying assumption that will be used for the one-dimensional case.

$$\frac{\partial^2 x}{\partial t^2} = -\frac{\mu}{m}\frac{\partial x}{\partial t} + \frac{L}{m}\left[\gamma(c(x+L/2)) - \gamma(c(x-L/2))\right] \tag{3}$$

The second differential equation, 4, describes the evolution of the camphor density, c. It is a reaction-diffusion type equation with moving, constant sources. The first term on the right side is diffusion with rate D. The second term represents loss through sublimation into the air and dissolution into the water bulk with combined rate k. The final term is the combination of sources on each of the N boats. Each source has a constant rate α over the area of the camphor disk. The position $\mathbf{x}_{\mathbf{r}i}$ refers to the center of the camphor disk. It is important to note that this most simple model does not include saturation of the camphor density, which may have significant consequences. Variations including saturation were also explored, and are described below.

$$\frac{\partial c}{\partial t} = D\left(\frac{\partial^2 c}{\partial x^2} + \frac{\partial^2 c}{\partial y^2}\right) - kc + \alpha\sum_{i=1}^{N} F(\mathbf{x} - \mathbf{x}_{\mathbf{r}i}) \tag{4}$$
$$F(\mathbf{x}) = 1 : \text{for } |\mathbf{x}| \leq \mathrm{r}_0,\ 0 : \text{otherwise}$$

To non-dimensionalize the 1-D equations, we define the following dimensionless quantities.

$$t' = t\frac{D}{L^2}\ ,\ x' = \frac{x}{L}\ ,\ c' = c\beta \tag{5}$$

Then the dimensionless parameters of the system become

$$\mu' = \frac{\mu L^2}{mD}\ ,\ k' = \frac{kL^2}{D} \quad , \quad \Gamma = \frac{L^3(\gamma_w - \gamma_c)}{mD^2} \tag{6}$$
$$r_0' = \frac{r_0}{L}\ ,\ R' = \frac{R}{L} \quad , \quad \alpha' = \frac{\alpha\beta L^2}{D}$$

Dropping the $'$ marks, the non-dimensional equations are

$$\begin{aligned}\frac{\partial^2 x_i}{\partial t^2} &= -\mu\frac{\partial x_i}{\partial t} + \Gamma\left[\frac{1}{c(x_i + \frac{1}{2})^2 + 1} - \frac{1}{c(x_i - \frac{1}{2})^2 + 1}\right] \\ \frac{\partial c}{\partial t} &= \frac{\partial^2 c}{\partial x^2} - kc + \alpha\sum_{i=1}^{N} F(x - x_i)\end{aligned} \tag{7}$$
$$F(x) = 1 : \text{for } |\mathrm{x}| < \mathrm{r}_0,\ 0 : \text{otherwise}$$

To approximate a realistic system, we mainly used parameters corresponding to the dimensional values: $R = 45cm$, $L = 0.6cm$, $r_0 = 0.15cm$, $m = 0.009g$, $\gamma_w = 72g/s^2$, $\gamma_c = 50g/s^2$, $D = 1cm^2/s$ unless otherwise stated. Other parameters were varied over realistic and unrealistic values in order to explore features of the model that are perhaps inaccessible to experiment. Also, collisions are considered inelastic to match the qualitative behavior seen in experiment.

2.3 Variations

There are many ways to refine the basic model to emphasize specific effects or to produce desired phenomena, but for theoretical investigations it is important to remember that the goal is not to construct a complex set of equations capable of

producing a predetermined result. Rather, the goal should be to examine the significant processes, model them, and if the results correspond to reality, explore their further consequences. The former is perhaps more of an engineering problem, though admittedly a very useful and important one, but I hope that the latter more closely resembles the aim of this research. Having said that, here are some variations on the basic model that were constructed with the hope of better reproducing experimental results.

2.3.1 Saturation

The basic model contains an intrinsic saturation point beyond which the camphor density can no longer increase. If the route were dense with sources, the density of camphor would approach a uniform value at which the rate of loss through sublimation and dissolution matched the addition from the source. From equation 4 this value would be $c = \alpha/k$. Since any practical system is not dense with sources, a more realistic distribution would have a series of peaks and the average would be less than this upper limit.

Alternatively, it is possible to impose a lower saturation value by modifying the source term to be dependent on the density. This approach was used, for example, in [21] and [28]. One reason for doing this is the ability to tune the system toward a desired part of the surface tension/camphor density relation. For example, one could set the saturation value to be at the steepest part of the curve. This is important if one is trying to use experimentally determined values for the parameters or trying to compute actual values for camphor density. Otherwise, it would be much simpler to merely modify the scaling parameter β in equation 2. Another reason to include saturation is that it changes the character of the distribution near saturated values. Since the loss through sublimation is slower when camphor density is limited, the distribution becomes smoother and the peaks around the sources are not as sharp as in the case of no saturation. This could have some effect on the interactions between boats.

To include saturation in the basic model, the function $F(\mathbf{x})$ in the source term of equation 4 can be replaced with a function such as in equation 8. This introduces the saturation value c_{sat} as a parameter, and the exponent m determines the shape of the saturation curve as shown in figure 3. Some simulations were run using various values for these parameters, but unless otherwise stated, the presented results did not include this saturation model.

$$F(\mathbf{x}, c) = 1 - \left(\frac{c(\mathbf{x})}{c_{sat}}\right)^m \text{ : for } |\mathbf{x}| \leq \mathrm{r}_0,\ 0 \text{ : otherwise} \tag{8}$$

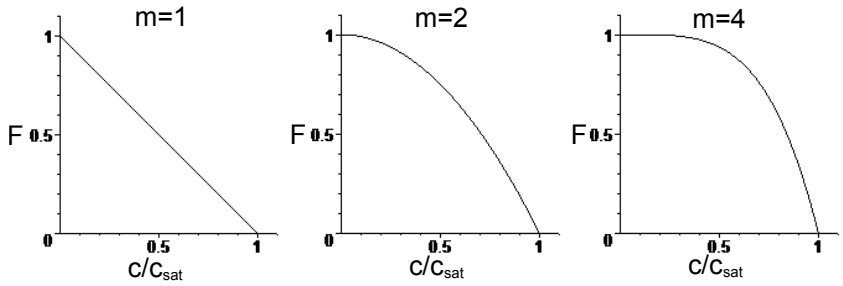

Figure 3: The modified source function $F(\mathbf{x}, c)$ vs. c/c_{sat} for $m = 1, 2, 4$.

2.3.2 Two-layer model

The two layer model was created to treat the camphor molecules on the water surface separately from those in the water bulk. The motivation for this is that camphor molecules diffuse much more rapidly on the surface of water than they do in the bulk. In simulation, very slow diffusion rates can result in intermittent motion and long memory of the camphor distribution. Faster rates are needed to produce quick interaction between boats at a distance.

This model requires two separate equations for describing the camphor density in each layer. Equation 9 for the surface layer and equation 10 for the bulk layer are similar to equation 4 from the basic model, but with several differences. The source terms must be modified because the surface layer only contacts the edge of the camphor disk and the bulk contacts the underside area of the disk. This can be further complicated by the effect of the plastic disk. The surface loss term needs to be separated into sublimation and dissolution parts because the dissolved camphor is added into the bulk layer. Similarly, the bulk loss term includes only a transfer of camphor to the surface layer. These interactions between layers require a number of new parameters which would be difficult to determine experimentally. In the end, this modification to the model creates a vast increase in complexity that has not been justified by its benefits. Although some simulations were run with this model, the results were not useful and are not presented here.

$$\frac{\partial c_s}{\partial t} = D\left(\frac{\partial^2 c_s}{\partial x^2} + \frac{\partial^2 c_s}{\partial y^2}\right) - k_1 c_s - k_2(c_s - c_b) + \alpha \sum_{i=1}^{N} F_s(\mathbf{x} - \mathbf{x}_i) \tag{9}$$

$$\frac{\partial c_b}{\partial t} = D\left(\frac{\partial^2 c_b}{\partial x^2} + \frac{\partial^2 c_b}{\partial y^2}\right) + k_3(c_s - c_b) + \alpha \sum_{i=1}^{N} F_b(\mathbf{x} - \mathbf{x}_i) \tag{10}$$

2.3.3 Non constant diffusion

As a simpler alternative to the two-layer model, consider the part of the surface beneath the plastic disk as part of the bulk. Set the diffusion rate in this region to be lower than in surrounding water. The most straightforward way of doing this is with a spatially discontinuous diffusion rate as diagrammed in figure 4. This approach was used in [29] to investigate the effect of diffusion distance on the motion of a single boat. Intermittent motion was a key feature observed. This model is used here to investigate intermittent motion in an ensemble of boats. Of course, the discontinuous diffusion rate requires careful selection of numerical methods for solving the camphor evolution equation. This model is the subject of current investigation, and meaningful results are not yet ready for presentation.

2.4 Numerical methods

The two differential equations in the basic model are of very different type and require different methods to solve. Also, one and two dimensional versions have some different requirements.

The simplest equation to solve is the one dimensional motion equation, 3. This can be written as a system of first order equations by introducing the velocity $v = \frac{\partial x}{\partial t}$. There are countless methods available to solve such a system. Since collisions are handled by manually adjusting the velocity and position of boats, multi step methods would be a poor choice. For simplicity, a fourth order Runge-Kutta method was used. Since the edges of the boat generally do not line up with the grid used for the camphor field, linear interpolation was used to determine c at the edges. This is reasonable since the camphor field is typically smooth on the

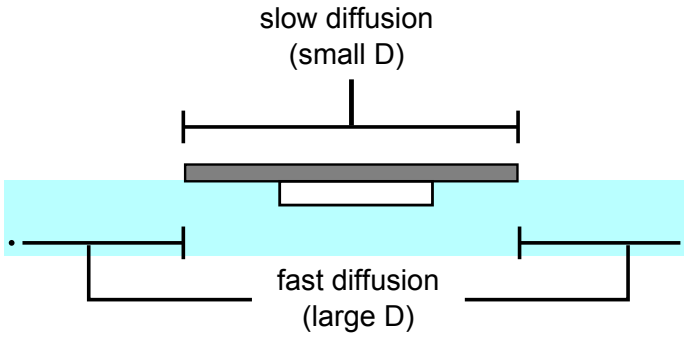

Figure 4: Slow diffusion beneath the boat corresponding to a bulk rate and fast diffusion everywhere else corresponding to a surface rate.

scale of the grid. Also, the Runge-Kutta method requires knowledge of c at a future time step. Unfortunately, solving for the future c also requires the future value of position. To acquire this, an approximation is made assuming c does not change during the time step. Later, when the future value of c has been properly computed, the position is recalculated. This iteration could be continued to refine the result, but for sufficiently small time steps the improvement would be insignificant.

The two dimensional motion equation is very similar and can also make use of the fourth order Runge-Kutta method. For computing the net surface tension vector, 128 evenly spaced points on the edge of the boat were used. Again, since the edge does not usually fall upon c grid points, bilinear interpolation was used.

The equation for the camphor density in one dimension, equation 4, requires more complex methods and takes the majority of the computation time. A common time stepping method used for diffusion equations such as this is the second order Crank-Nicolson method, which was used here. A second order, centered, finite difference method was used to discretize the spatial derivative on the right side. Since the equation depends on the positions of the boats at the next time step, the motion equation was incremented first. In two dimensions, a second order alternating direction implicit(ADI) method was used. This method shares many features and requirements with the one dimensional Crank-Nicolson method. Both the one dimensional Crank-Nicolson and two dimensional ADI methods are unconditionally stable, and the discretization was chosen to satisfy $D\frac{\Delta t}{\Delta x^2} < 1$ to maintain accuracy.

3 Results

3.1 Regarding spatio-temporal diagrams

Spatio-temporal diagrams are used throughout this section to display the trajectories of boats in a one-dimensional system. Here is a brief description to aid in reading such diagrams. The example in figure 5 has a vertical time axis with time increasing in the upward direction. The horizontal axis represents position along the periodic, one-dimensional route. Unless otherwise stated, all diagrams will use these axes. The lines correspond to the position of a boat as it evolves in time. Therefore, a line with shallower slope corresponds to a more quickly moving boat and a vertical line corresponds to a stationary boat.

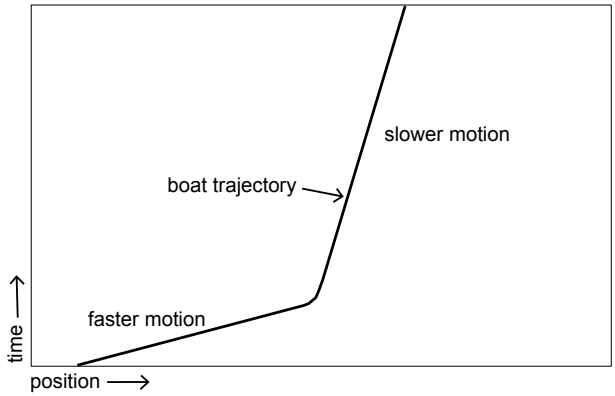

Figure 5: Example spatio-temporal diagram with labels.

3.2 1-D asymmetric boats

3.2.1 Description and background

The results described here were first presented in [5]. The asymmetry of a boat refers to the non-concentric placement of the camphor disk on the plastic disk. Unless otherwise stated, the center of the camphor disk is aligned with the edge of the plastic disk. This grants the boat a preferred direction of travel because the side closest to the camphor will typically experience a higher camphor density than the opposite side. A group of these boats are oriented in the same direction in a one-dimensional channel. The motivation for this configuration is to create a system resembling traffic flow such as vehicles on a road, ants moving along a trail, or pedestrians on a narrow path.

Some of the first experimental work concerning collective motion of asymmetric boats in a channel is described in [28] and [1]. This clearly demonstrated interaction between two boats and its influence on their motion. Larger numbers of boats were then used in [4] and [5], where more complex dynamical patterns were observed. A free flowing, almost homogeneous distribution was seen for smaller numbers of boats. As the number was increased beyond some threshold, congestion appeared with the formation of a jammed region in which boats traveled more slowly and closer together. This congestion looks qualitatively very similar to that seen in highway traffic. A third type of motion was also observed in which boats clustered together into groups and traveled in a steady formation. This behavior is labeled clustering. These three types of motion are shown in figure 6. Some analytical work was done in [4] to explain the formation of a congested state. The focus of this work is the clustered state.

The clustering behavior seen in both experiment and simulation appears very similar to observations of ants marching in a line. As described by John *et al.* [30], a line of ants may form what they called platoons, which are stable, high density groups of ants moving at a constant speed. Individual ants following behind the platoon sense its pheromone trail and may move at a higher velocity due to the strength of the trail. This allows the individual ants to catch up with and join the group. Clusters of camphor boats are also stable, high density groups that travel at constant speed. By a mechanism described below, the trail of camphor left by the cluster causes following individuals to travel at higher speed and catch up with the cluster. Although camphor boats are not sentient and are driven by much simpler principles, these behaviors bear many similarities.

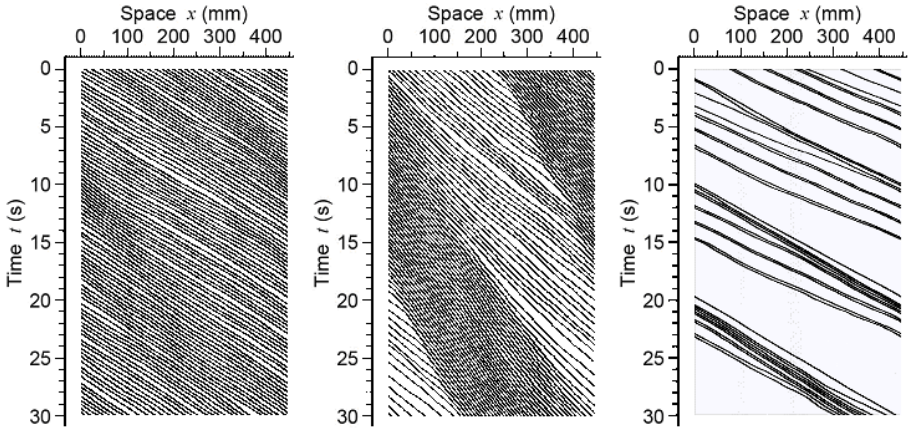

Figure 6: Spatio-temporal diagrams of experimental data showing a)free flow, b)congested flow and c)clustering. Note that the time axis is increasing downward in these diagrams.

3.2.2 Results of simulation

Each of the three experimentally observed patterns can be reproduced in simulation. Examples of simulated results are shown in figure 7. Each parameter in the model was varied and their influence on the collective motion was examined. Although each parameter had some noticeable effect on the behavior, there were a few that primarily determined the type of flow. The source rate α, the loss rate k, and the number of boats N are the parameters that will be mainly discussed here since they are most closely related to clustering. The camphor radius r_0 and the route length have similar effects, but can be related to α and N as determining the amount of camphor added to the system and the total boat density respectively.

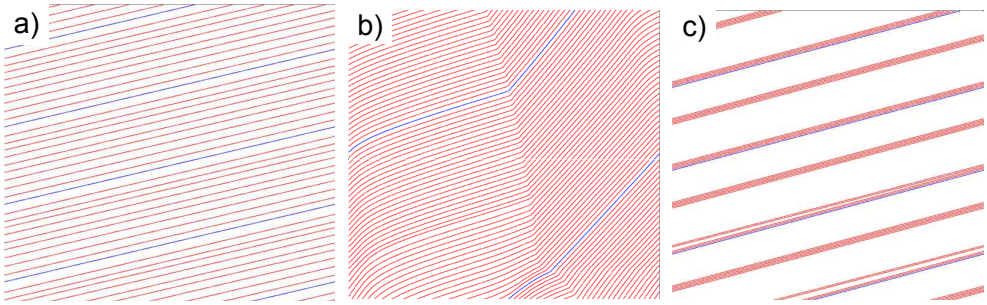

Figure 7: Results of simulation showing a)free flow, b)congested flow and c)clustering. The blue trajectory is just a visual aid.

The clustered state in simulation is qualitatively very similar to that from experiment. Even the formation of a cluster from an unclustered state appears similar as shown in figure 8. Due to some similarities between a clustered state and a congested state, it is important to quantitatively differentiate them. The following quantity is useful as an order parameter because it measures the compactness and stability of clusters.

$$b = \max_{i=1..N} \frac{\langle d_{fi} - d_{bi} \rangle}{R - NL} \tag{11}$$

Here d_{fi} and d_{bi} are the distances from the next boat in front and in back of boat i respectively, and the normalizing factor $R-NL$ is the total empty space in the route.

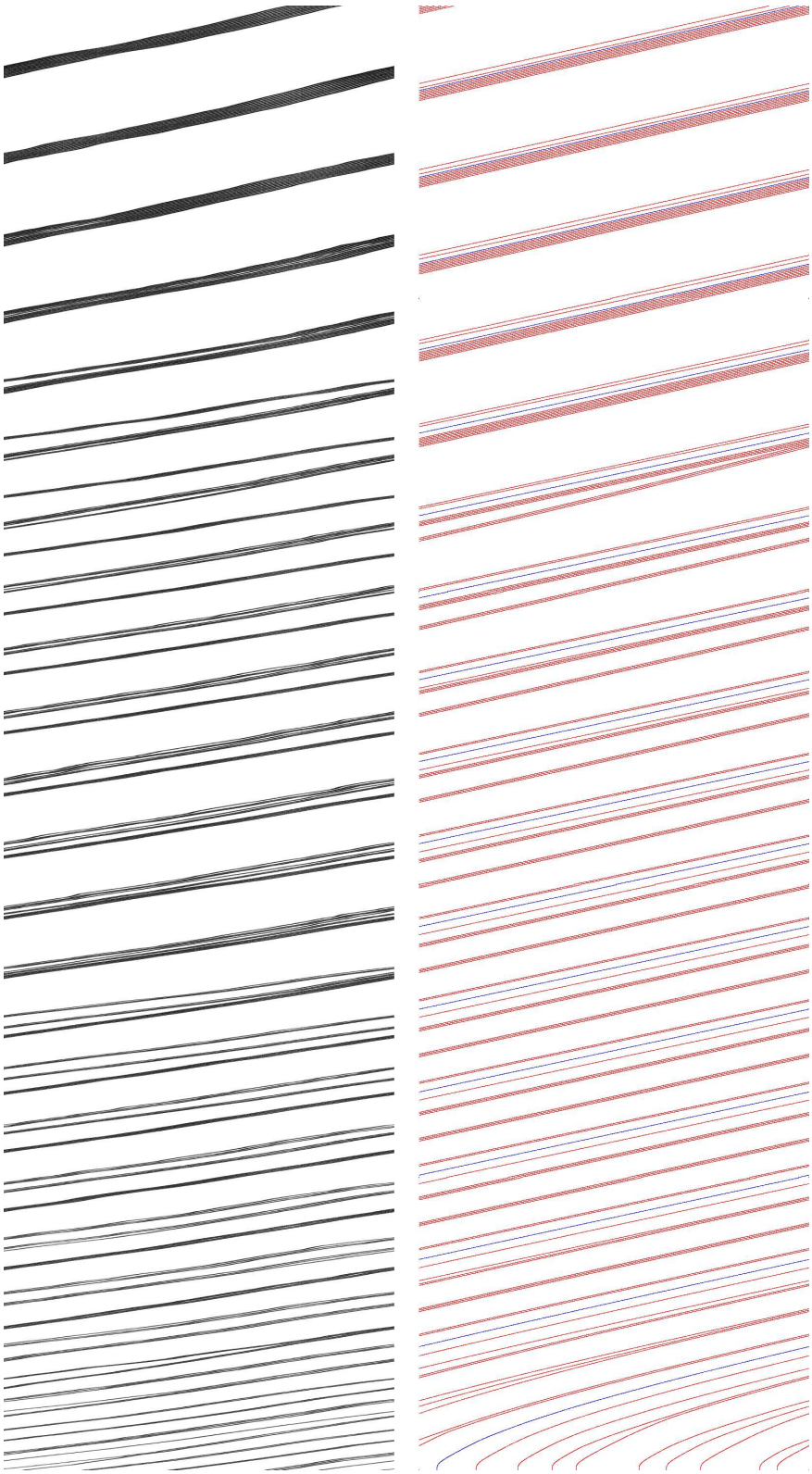

Figure 8: *(left)*Experimental data and *(right)*simulation results showing the formation of a cluster from an unclustered condition.

The brackets represent a time average. For a system containing one cluster with all boats in contact, $b = 1$. For ideal homogeneous flow, $b = 0$. For jammed flow, b will approach zero when averaging over long time intervals. In practice, particularly in experiment, b may deviate from these values, but should generally be much larger for the clustered mode.

Using the value b it is possible to explore the parameter dependence of clustering. Figure 9.a shows the value of b in the (k, α) parameter space. The linear trend of the transition between clustered and non-clustered states is very clear. Considering that these parameters represent the loss and source rates, this result suggests that the transition may occur at a certain equilibrium value for the average camphor density in the route. The (k, N) parameter space shown in figure 9.b is somewhat different. Again the transition appears to occur at higher values of N with increasing k, but the curve seems to approach some maximum value of N above which clustering is not seen. An explanation for this is given further below.

Another interesting feature seen in figure 9 is the very abrupt transition between clustered and non-clustered states. To check for hysteresis, the values of α and N were gradually increased and then decreased across the transition. The system was given time to approach a steady state between each measurement and the results are shown in figure 10. The hysteresis is very clear for both transitions. For larger values of k, however, the hysteresis with respect to α vanishes. This suggests a change from a subcritical to a supercritical bifurcation.

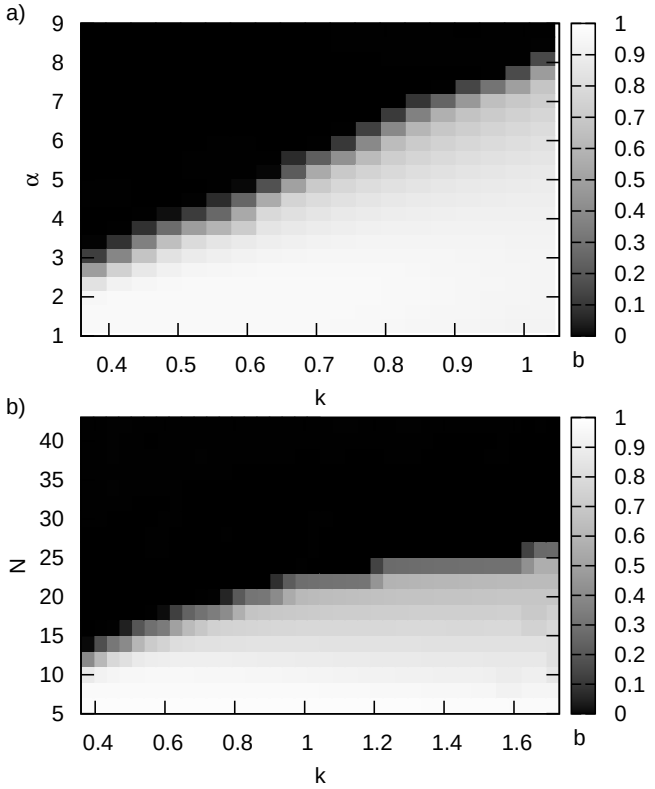

Figure 9: a) b changes abruptly at particular values of k and α. b) There is a maximum value of N, dependent on various parameters, above which clusters do not form. The other dimensionless parameters used here are $\mu = 0.24$, $\Gamma = 528$, $R = 75.8$, $r_0 = 0.25$.

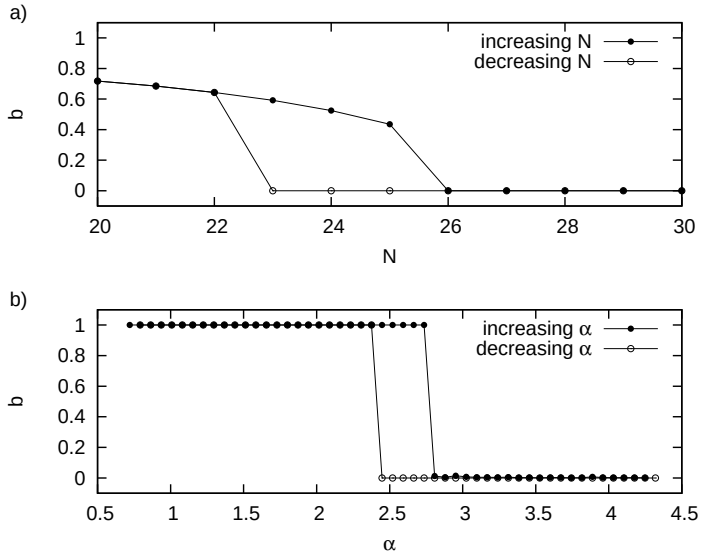

Figure 10: Hysteresis is seen by gradually increasing and decreasing N ($k = 0.73$) and α ($k = 0.36$). For $k = 0.73$, the hysteresis with respect to α vanishes. Other parameters as in Fig.9.

3.2.3 Analysis

The mechanism responsible for the clustering behavior can be found by examining the model, specifically in the surface tension formula $\gamma(c)$ rewritten here for convenience.

$$\gamma(c) = \frac{\gamma_{water} - \gamma_{camphor}}{(\beta c)^2 + 1} + \gamma_{camphor} \tag{12}$$

For camphor density less than a critical value, $c_t = 1/(\sqrt{3}\beta)$, the slope of $\gamma(c)$ becomes steeper with increasing c. In other words, the magnitude of $\frac{d\gamma}{dc}$ has a peak at c_t. This is shown in figure 11.a. To relate this to the motion of boats, if the average camphor level around a leading boat is lower than around trailing boats, the leading boat may feel a weaker driving force. The trailing boats would then move at a higher velocity and approach the leading boat.

We can easily apply this idea to the case of two boats. First, assume that the boats are moving with constant velocity, v, and that the camphor field in the moving reference frame of the boats has reached a steady state. The camphor field then satisfies the traveling pulse equation, 13, where v is the constant velocity and x_0 is the constant position in the moving reference frame.

$$-v\nabla c = \Delta c - kc + \alpha F(x - x_0) \tag{13}$$

Solutions to this equation for the case of symmetric boats are given in appendix A, and similar solutions can be found for the asymmetric case as well. The details of the solution are not important here as we will only examine their qualitative features. Some example solutions are shown in figure 11.b. The dashed line is the solution for one boat and the solid line is for two boats traveling to the right. Note the higher concentration around the left peak in the two-boat curve. This feature remains even if the boats are placed close enough to be in contact. By the mechanism described above, if $c < c_t$, the two boats will approach each other and travel in a close configuration. If additional boats are added to the system, they will be gathered into the cluster through the same mechanism. This leads to the question of whether the cluster remains stable as the number of boats increases.

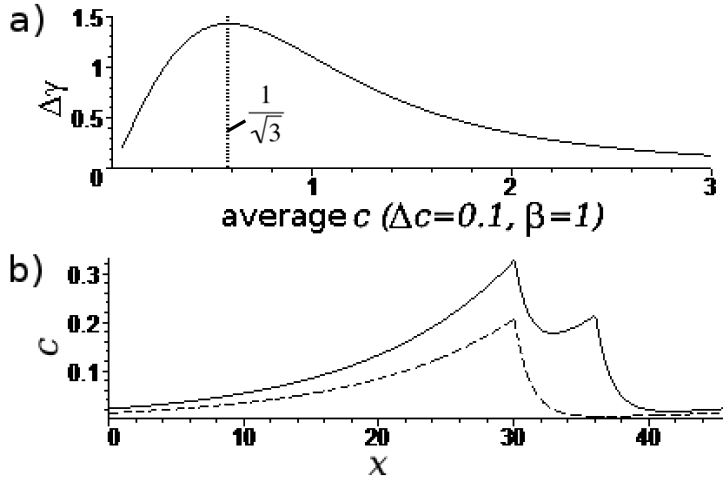

Figure 11: a) $\frac{d\gamma}{dc}$ increases with increasing average c up to $c_t = 1/(\sqrt{3}\beta)$. b) Steady state $c(x)$ for one boat(dashed) and two boats(solid) moving at constant velocity to the right. The peaks approximate the rear edges of the boats, which have length 0.6

To test for stability, we can vary the distance between the trailing boat at the back of the cluster and the next forward boat. Solving equation 13 with this configuration, it is possible to compute the net force on the trailing boat relative to that of the next forward boat. A positive force will cause the trailing boat to accelerate and move closer to the next boat. Conversely, a negative force will cause it to move further away. The result of such a calculation is shown in figure 12. The region in which a stable cluster will form extends from zero distance out to several boat lengths(approximately 8.4 in the figure). This wide region provides stability against reasonable perturbations and ensures that a cluster can form even from more dispersed configurations.

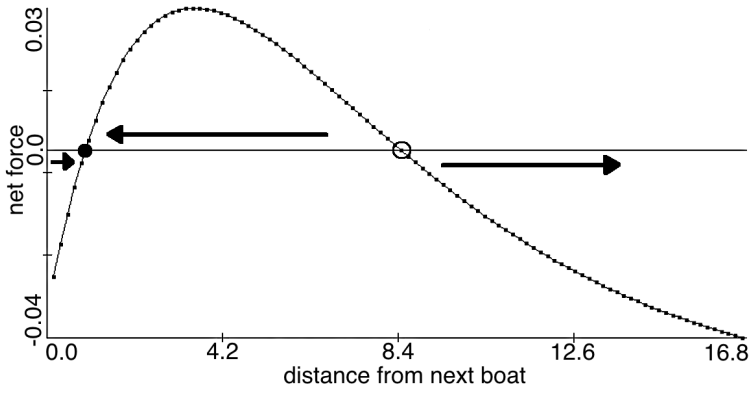

Figure 12: Net force on the last boat vs. its distance from the next forward boat. A positive force will decrease the distance. The solid dot represents a stable fixed point, and the hollow dot an unstable fixed point.

The result shown in figure 12 also shows the equilibrium distance at a finite separation rather than in contact. This is not always the case. For some parameter

values, the net force remains positive even at zero separation distance. This would cause the boats to move in fixed contact.

In addition to the average value of c being lower than c_t, the number of boats in the system can also have an affect on clustering. If the size of the cluster becomes comparable to the total route length, the boats at the back of the cluster will influence the boats at the front. In other words, the trailing boat will provide a boost for the leading boat. If the effect is strong enough, it will pull the cluster apart. Testing this idea in simulation showed this to be the case. Boats can be gradually added to a stable cluster up until some maximum value. Adding one more boat will cause the cluster to disintegrate and form a homogeneous flow state. For the parameter space tested, the maximum number of boats to form a cluster was always less than the critical value needed to form congestion. Thus, at least for this parameter space, clustering and congestion did not coexist, but the possibility should not be ruled out.

3.3 1-D symmetric boats

3.3.1 Description and background

The results described here were first presented in [6]. This type of boat contains a camphor disk placed concentrically on the plastic disk so that there is no preferred direction of travel. The ensemble is set up similar to the asymmetric case described above. Under ideal conditions, a single boat or homogeneous distribution of boats will remain stationary in an unstable equilibrium. Of course, in any practical situation there are numerous influences that will break the delicate symmetry. Experimental work is currently under way, but at this time there are no published results corresponding to the simulations described here. It is hoped that such experiments will soon be conducted to test the validity of these theoretical results.

3.3.2 Results of simulation

Three distinct types of behavior were observed in which the boats are *a)*stationary, *b)*repeatedly alternating direction, or *c)*flowing in one direction. The key parameters determining the type of motion are the viscosity of the water and the density of boats. Viscosity is determined by the parameter μ in equation 4. Boat density is given here as the fraction of route length occupied by boats, so a density of 1.0 means the route is densely packed with boats. Two order parameters are used to quantify the different phases, the root mean square velocity $\sqrt{\langle v^2 \rangle}$ and the magnitude of the mean velocity $|\langle v \rangle|$. The brackets mean averages over both time and the ensemble. Furthermore, the results of several(10 or 20) separate simulations are averaged to produce the values presented. These time averages are taken over a long interval($\Delta t > 800$), corresponding to hundreds of oscillation periods. Measurement begins after an initial relaxation period to reduce transient effects. Typical short oscillation periods were around 1 unit of time, but some irregular oscillations close to the flow transition took much longer and required longer measurement intervals. Each parameter value is given a fresh system containing boats with stationary, randomized initial conditions.

The following are qualitative descriptions of each phase listed in order of decreasing viscosity. It will be useful to refer to the example spatio-temporal diagrams in figure 13 and the phase diagram in figure 14.

(I). In the very high viscosity phase, the system approaches a stable, stationary equilibrium in which the boats are uniformly spaced. Nothing is moving, so $\sqrt{\langle v^2 \rangle}$ and $|\langle v \rangle|$ are both zero.

(II). As the viscosity is decreased, there is a critical value labeled μ_{c1} below which the boats begin to move. This results in a non-zero value of $\sqrt{\langle v^2 \rangle}$ as shown

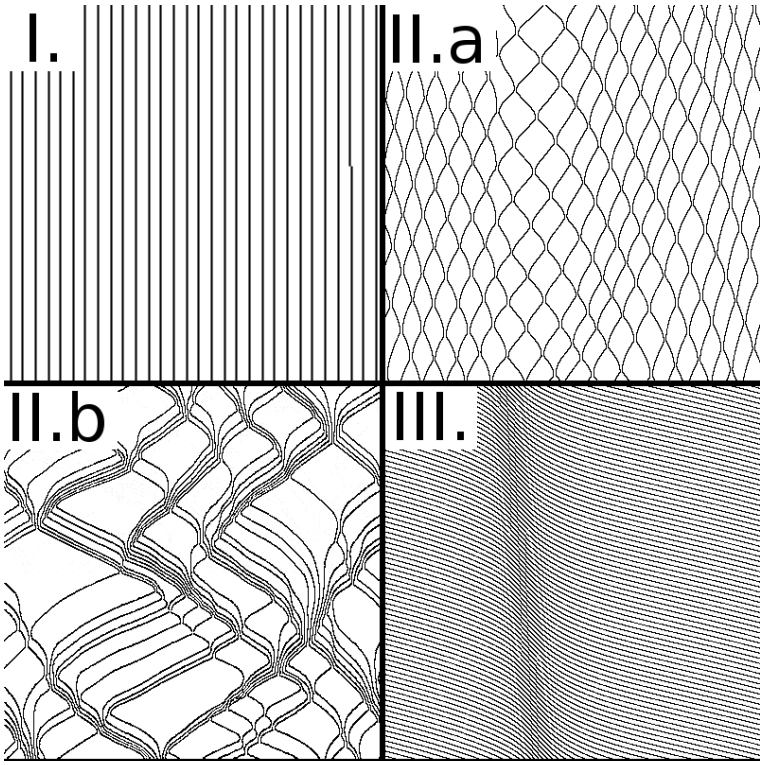

Figure 13: Spatio-temporal diagrams showing I) stationary phase, II.a) synchronized oscillation, II.b) erratic oscillation, III) unidirectional flow. Note the left moving dense region in III representing congestion.

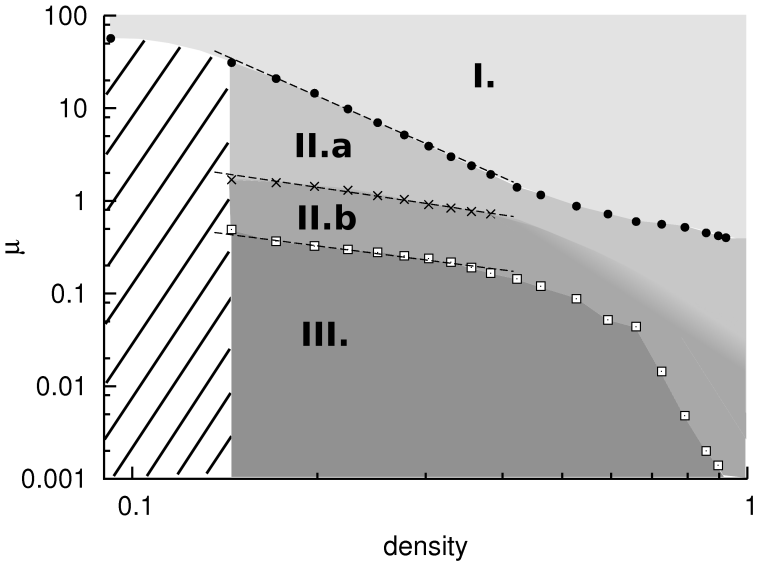

Figure 14: Phase diagram for the types of behavior. The dashed lines are a power law fit for densities between 0.17 and 0.38, but such a relation is not implied. Other parameters are: $k = 0.072$, $\Gamma = 528$, $\alpha = 7.2$, $r_0 = 0.25$, $R = 75$, $N = 20$.

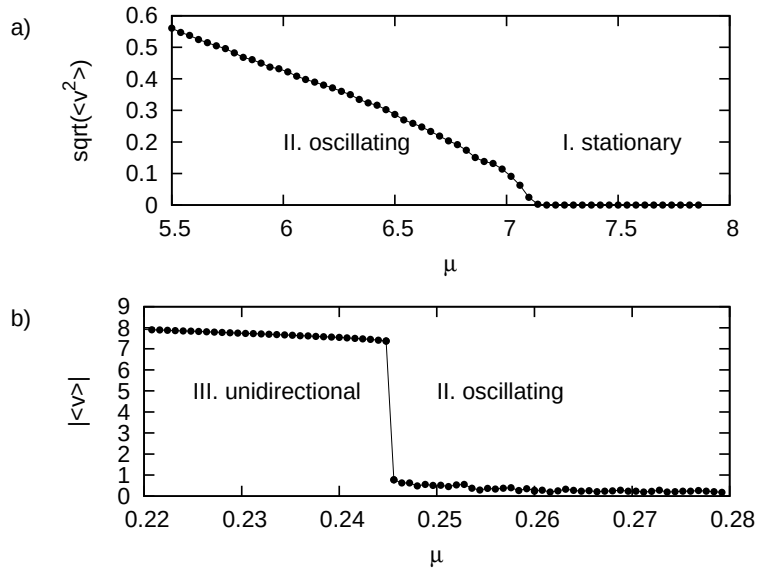

Figure 15: a) $\sqrt{\langle v^2 \rangle}$ in the vicinity of μ_{c1}. b) $|\langle v \rangle|$ in the vicinity of μ_{c2}. Same parameters as fig.14

in figure 15. The motion is oscillatory meaning that the boats repeatedly switch direction. On average there is still no preferred direction of travel and the boats spend roughly equal amounts of time moving left and right, corresponding to a zero value for $|\langle v \rangle|$. For boat densities below about 0.15, the type of motion depends heavily on initial conditions and oscillation may not be seen, but the change in $\sqrt{\langle v^2 \rangle}$ at μ_{c1} remains valid.

A closer look at the motion reveals two very different types of oscillation. Several diagrams are given in appendix B to show the typical oscillatory patterns. Higher viscosity values result in a very regular, synchronized movement labeled as **(II).a** in figures 13 and 14. The degree of synchronization between boats can be measured using the cross correlation of their velocities. This quantity, labeled simply as correlation, is given by equation 14. It is shown in figure 16 as a function of distance in numbers of boats(i.e. a distance of 1 means the next boat in the route). A correlation of 1 means the boats have identical velocity and -1 means their velocities have the same magnitude, but are in opposite directions. A correlation of 0 means the boats are on average unsynchronized. Introducing a lag value in the cross correlation would reveal synchronization with phase differences, but for this work only the zero lag value is considered. Figure 16.a and 16.c correspond to type II.a behavior. Note the strong pattern of alternating negative and positive values meaning that neighboring boats are oscillating roughly 180 degrees out of phase. This pattern becomes weaker at larger distance.

$$correlation(n) = \left\langle \left\langle \frac{(v_i - \overline{v})\,(v_{i+n} - \overline{v})}{\sigma_i \sigma_{i+n}} \right\rangle_i \right\rangle_{time} \tag{14}$$

When viscosity is lowered further, the oscillations become irregular and appear chaotic. This is labeled as **(II).b**. Despite the chaotic appearance, the computed Lyapunov exponents still converge to zero meaning that the motion is not officially chaotic. The correlation shown in figure 16.b and 16.d reveals a complete lack of the synchronization pattern from II.a. The transition from II.a to II.b behavior is not sharply defined, especially for high density. The values shown in figure 14 are the points at which the correlation of neighboring boats increases to zero and

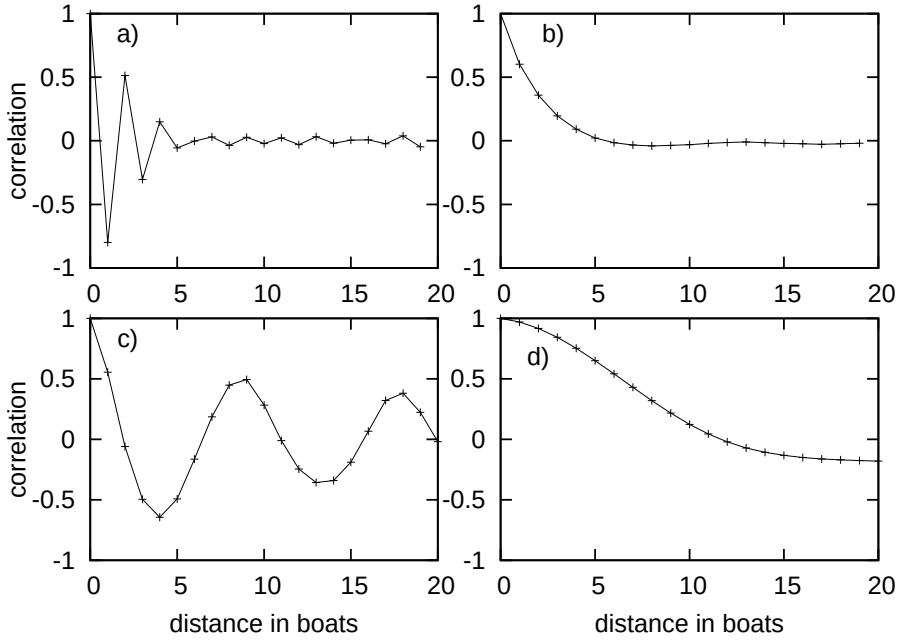

Figure 16: Cross correlation of velocity vs. distance in boat numbers for a) density=0.26, $\mu = 0.6$ b) density=0.26, $\mu = 4.0$ c) density=0.6, $\mu = 0.12$ d) density=0.6, $\mu = 0.68$. a) and c) correspond to type II.a, while b) and d) correspond to II.b.

roughly approximates the qualitative change in behavior. Again, it is instructive to look at the additional diagrams in appendix B to see the change from correlated to uncorrelated oscillations. Decreasing viscosity further causes the period of oscillation to grow much larger. Groups of boats, sometimes containing all the boats in the system, travel together in the same direction, then spontaneously reverse. Given sufficient time, the value of $|\langle v \rangle|$ still approaches zero.

When the boat density is very high, the character of the oscillatory motion is different. High density II.a motion, shown in figure 17.a, still shows a strong synchronization pattern, but rather than neighboring boats moving out of phase, the antisynchronized boats may be further away. Figure 16.c illustrates this kind of synchronization. High density II.b motion, shown in figure 17.b, also lacks the synchronization pattern as shown in16.d. Despite their slightly different character, these two types of motion contain the same defining features as the low density versions, so they do not need to be labeled separately.

(III). Below a second critical value, μ_{c2}, the boats no longer reverse direction and they all flow together in one spontaneously chosen direction. This breaking of symmetry appears as the discontinuity in $|\langle v \rangle|$ shown in figure 15. To test for hysteresis in the discontinuity, viscosity was gradually increased and decreased using several values of density. For the parameter space tested, no hysteresis was observed. This kinetic phase transition is similar to the behavior of some kinds of self propelled particles [7, 8, 9, 10].

There are several types of flow seen within phase III. Some of these closely resemble the results described previously for asymmetric boats such as homogeneous free flow, congestion and clustering. Pulsing flow, in which localized congestion periodically appears was also observed. The parameter dependence of these different types of flow were not extensively explored.

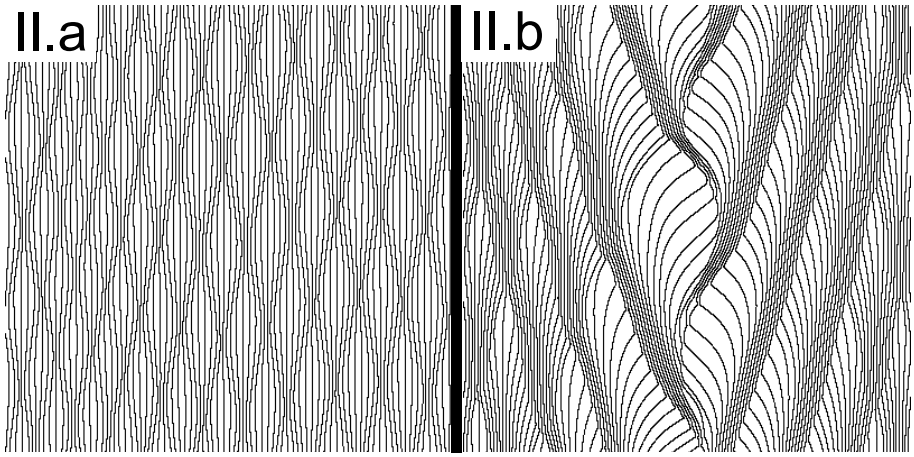

Figure 17: High density versions of II.a and II.b motion. Density = 0.6.

3.3.3 Analysis

The transition between stationary and moving phases, I to II, can be understood by considering the motion of one boat. A detailed analysis was done by Nagayama *et al.* [20] for the case of a bare camphor pellet in one dimension. The essential parts are described here and extended to the case of a camphor boat. First, assume that the boat has reached an equilibrium speed, ignoring the possibility of intermittent motion. The camphor field is then time independent in the moving frame of the boat. It satisfies the traveling pulse equation, 15, where v is the constant velocity and x_0 is the constant position in the moving reference frame.

$$-v\nabla c = \Delta c - kc + \alpha F(x - x_0) \tag{15}$$

The details of the solution for the case of a camphor boat containing a plastic disk can be found in Appendix A. This result includes a bifurcation between a stable stationary solution and a nonzero constant velocity solution. Moreover, the bifurcation can be supercritical or subcritical depending on either the source rate α or the radius of the camphor source r_0. It is supercritical for small values of α or r_0 and subcritical for large values. The results of analytical calculations and their corresponding simulations are shown in Figure 18. This result can be extended to a uniformly spaced ensemble of boats by shrinking the periodic domain to include exactly one boat. Unfortunately, it is only valid if all boats are moving identically, which does not match the oscillatory behavior observed.

To explain the oscillatory behavior, there must be an effective repulsive force acting on boats that are close together. This can be understood by examining a simple scenario. First assume that two boats in the system begin moving toward each other, and that their initial separation is sufficient that they can approach equilibrium velocity before colliding. Because their speeds are nearly equal, and the collisions are modeled as inelastic, the boats will almost come to a stop after colliding. Also, assume that the relaxation time of the local camphor field is sufficiently short compared to the motion of the boats. While the boats are close together, the camphor field will have the form of two neighboring peaks with exponentially decreasing sides. Due to the contribution of each camphor source, the concentration directly between the peaks, corresponding to the closer edges of the boats, will be higher than that at the further edges of the boats. The higher surface tension on the further edges will provide an effective repulsion. The repulsion does not need to have a long range, because once a boat is moving in one direction, it will tend

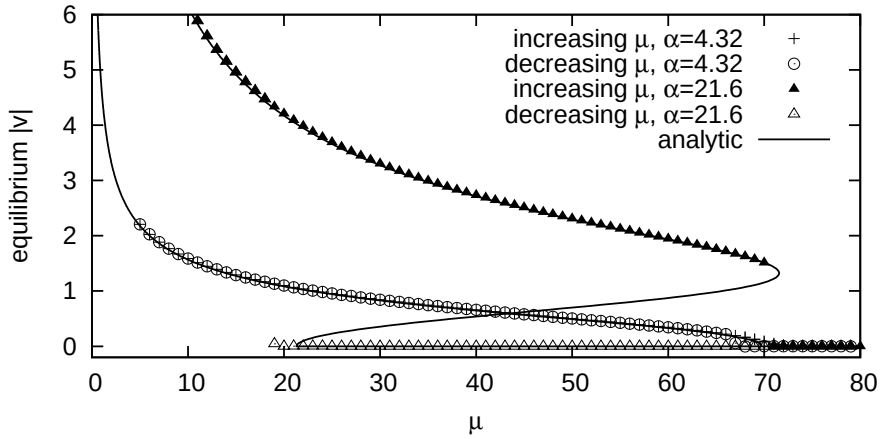

Figure 18: Analytical solutions(solid lines) and their corresponding simulation results(markers) for the equilibrium velocities at a given viscosity. Includes both subcritical and supercritical bifurcations.

to continue in that direction. This process describes the regular oscillation seen in II.*a*. However, if the velocities of the two boats are significantly different, the final velocity after colliding may be large enough that both boats will begin traveling in the same direction. The exact speed difference required would depend sensitively on the local camphor profile and system parameters. This sensitivity may explain the seemingly chaotic oscillation patterns seen in II.*b*.

The transition between flow and oscillation cannot be treated by such simplifications because the collective behavior is extremely complicated and collision effects are significant. Instead, I will outline a possible scenario based on observations, and leave it to the reader to judge the validity of this interpretation. Consider a single boat in the ensemble. The camphor field influencing it can be approximated as a combination of the boat's local field generated by its camphor disk and a large-scale field generated by the whole ensemble. The local part typically has the shape of a sharp, localized peak, while the large-scale part is much smoother and varies on the scale of the entire route. Using these two parts, the driving force can then be separated into local and large-scale parts. The local part typically propels the boat in the direction of its velocity, while the large-scale part may act in either direction depending on the structure of c. We will define f_l as the component of the force generated by a boat's local field. f_g is the component generated by the large-scale field.

Assume that f_l is constant, and that $f_g(x,t)$ depends on the large-scale profile of $c(x,t)$ which may change in time. A boat is moving with velocity v. Then the condition $f_l + f_g(x,t) < \mu v$ will cause the boat to slow down. Recall that the driving force depends on the difference in c between the two sides of the boat and acts in the direction of decreasing concentration. This means that if a boat is moving toward an increasing gradient in c, f_g will be negative and the boat may slow down. Such a condition is often created by a boat density peak such as seen in congested flow, which generates a peak in c. In the flow phase, the boat's momentum is enough to overcome the opposing gradient as it approaches the peak. If the viscosity is increased, the boat will have a lower speed, and may stop and reverse direction before reaching the peak. This reversal happens repeatedly for viscosity above μ_{c2}, causing oscillation. Note that the boats may pass the peak several times or collide with other boats before finally reversing direction.

3.4 2-D symmetric boats

3.4.1 Description and background

A circular dish containing several circular camphor disks was studied by Soh *et al.* [27]. They found that small numbers of boats moved randomly, but as the number of boats increased, they began to interact in interesting ways. With seven or more boats in the dish, the motion became more synchronized. The boats seemed to move in a steady formation. With many more boats in the dish, the boats became somewhat crowded and the effect of the walls became significant. Finally, at 47 boats, the ensemble became frozen into a very regular lattice. This transition may be closely related to the transition between moving and stationary phases described in the previous section. In fact, the phase diagram in figure 14 shows that for a fixed viscosity, a transition from uncorrelated motion to correlated motion and finally to a homogeneous stationary state may be achieved by increasing the density of boats. However, that result is for a one-dimensional system and it is not clear whether that behavior can be generalized to two dimensions.

3.4.2 Results of simulation

This is a subject of current research and there are few complete results, but some preliminary observations are described here. The most notable is the existence of a globally ordered stationary state that appears very similar to experimental results. Since there are now two spatial dimensions, the three-dimensional spatio-temporal diagram is not as useful for visually interpreting the qualitative behavior. Instead, snapshots of the configuration, including force vectors and a colored surface tension gradient, will be used. This provides an intuitive visual for understanding the qualitative behavior. The force vectors and surface tension gradient in the figures are both normalized, so the fluctuations may appear large even though their magnitude is very small. See the color scales below the figures for reference.

Figures 19-21 show the typical behaviors for a given parameter set with different numbers of boats. In figure 19, the density of boats is small and the boats are moving freely according to the constantly changing surface tension gradient. There is no order in their configuration or correlation in their motion. Figure 20 shows a slightly higher density of boats for which the boats are again moving freely. Reliable quantitative evidence has not yet been computed, but visual analysis seems to hint at a correlation in the motion. Boats that are in close proximity tend to travel in almost the same direction. Looking at the figure, it is possible to isolate several groups of three or four boats that are driven in the same direction. The reason for this is clearly seen in the colored surface tension gradient. The major structure in the surface tension is on a larger scale than the size of individual boats. In other words, an area of high surface tension may be broad enough that several nearby boats are drawn toward it simultaneously. The figure shows such a region in the center that is pulling in many of the boats from all sides. It is important to remember, however, that these are only visual interpretations and a more rigorous analysis has not yet been made. Finally, figure 21 shows a high boat density for which the boats are all nearly stationary. As discussed in [27], the boats begin to feel the confinement of the walls. There is a slight repulsive force between boats and between a boat and the wall, which effectively dampens the motion of boats and causes them to spread out almost homogeneously. The force vectors and surface tension gradient in the figure are both normalized, so the fluctuations may appear large even though their magnitude is very small and the boats are essentially stationary.

Looking at the surface tension color scales reveals another important effect. Naturally, when there are more boats the average camphor density is higher. If the value is typically much larger than $\frac{1}{\beta}$, the variation in surface tension will be very small

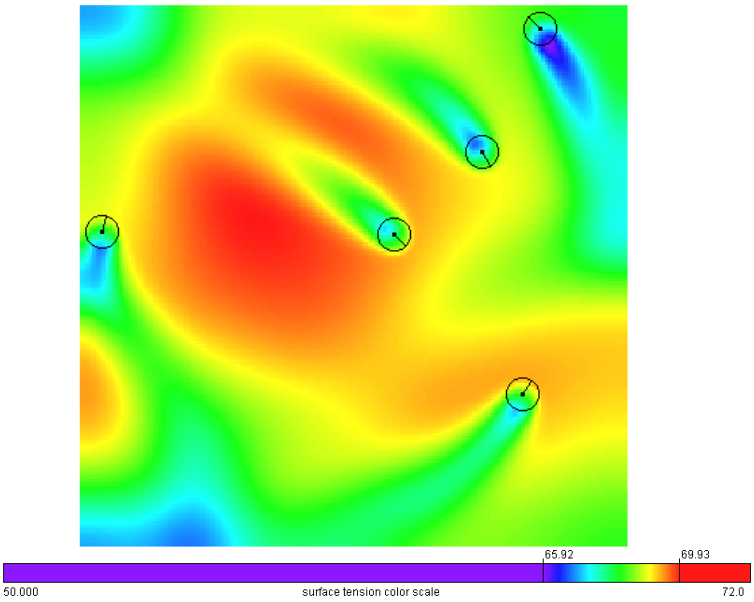

Figure 19: Snapshot of simulation with $N = 5$. The black circles represent the boats. The black lines inside the circles show the direction of the driving force. The color represents the normalized surface tension. The parameters are: width= $5cm$, $L = 2r_0 = 0.3cm$, $D = 0.1cm\ s^{-2}$, $k = 0.1s^{-1}$, $\alpha = 10$, $\mu = 0.1g\ s^{-1}$, $\beta = 0.33$

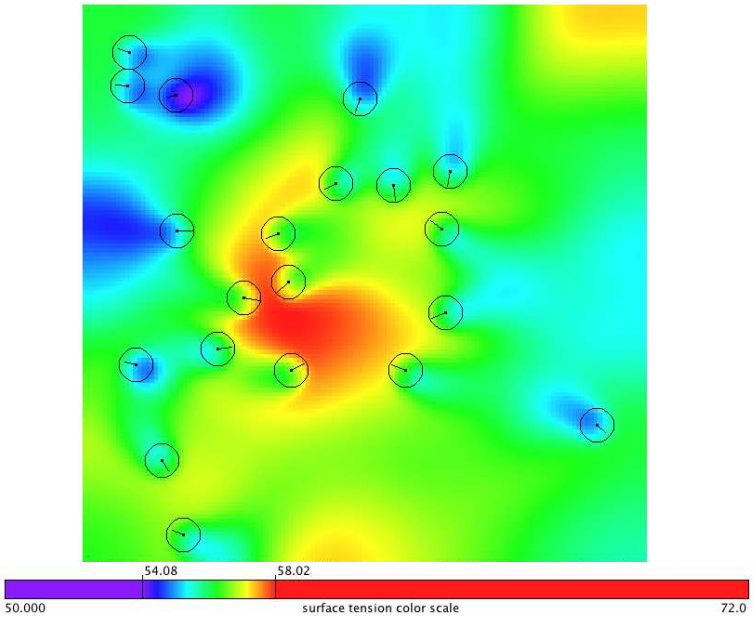

Figure 20: Snapshot with $N = 20$ and parameters same as figure 19.

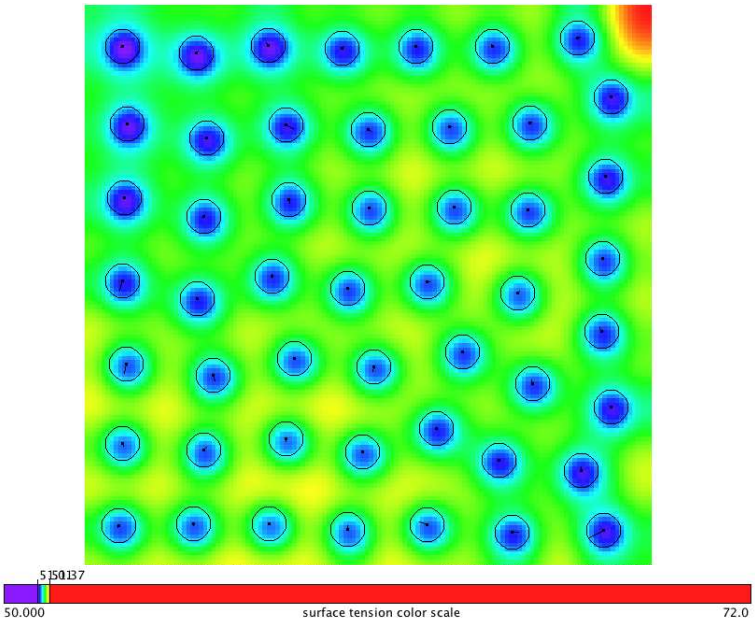

Figure 21: Snapshot with $N = 50$ and parameters same as figure 19.

even if the camphor density varies significantly. This means that driving forces on the boats will be small. Although this may be a key process in the formation of the stationary state, it is worthwhile to try excluding this effect by including camphor saturation in the model as discussed in section 2.3.1. The saturation value was at $\frac{3}{\beta}$ and the number of boats was varied as before. The stationary state did occur, but at a boat count of 90, which is much larger than for the case of no saturation.

A second interesting observation is a temporary periodic clustering. This occurs for the medium boat density discussed in the previous paragraph. As mentioned, the structure in the surface tension is typically larger than the size of boats, so a region of high surface tension may attract several nearby boats. These boats converge on the surface tension peak forming a temporary cluster of boats. As the camphor coming from the clustered boats decreases the surface tension in this region, the boats are pulled into surrounding water and the cluster is dispersed. This process repeats itself in various locations and with varying intensity. Figure 22 is a snapshot of such a situation. The time averaged pair distribution function in equation 16 was used to quantify the behavior, giving the result shown in figure 23. Here ρ is the total boat density and $V(\mathbf{x}_i, r)$ is the volume of a circular shell around boat i with radius r and width δr including only the portion lying within the square domain. The function $\delta(r_{ij} - r)$ equals one if boat j is within the shell and zero otherwise. $g(r)$ shows a strong peak at a distance of about 0.3, which is equal to the boat diameter. This corresponds to boats that are in contact with each other. Since this value is averaged over a relatively long time, random motion would give $g(r) \approx 1$ for all distances larger than the boat diameter. This means that the motion is certainly not random.

$$g(r) = \left\langle \frac{1}{N\rho} \sum_i \frac{1}{V(\mathbf{x}_i, r)} \sum_j \delta(r_{ij} - r) \right\rangle_{time} \tag{16}$$

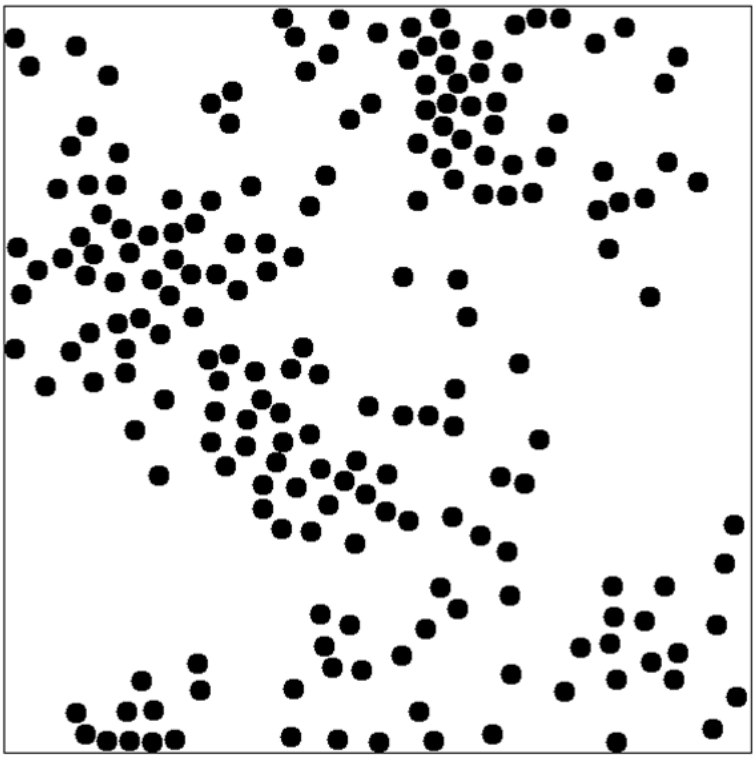

Figure 22: Snapshot showing temporary regions of high boat density. Surface tension is not shown to more easily see the boat configuration.

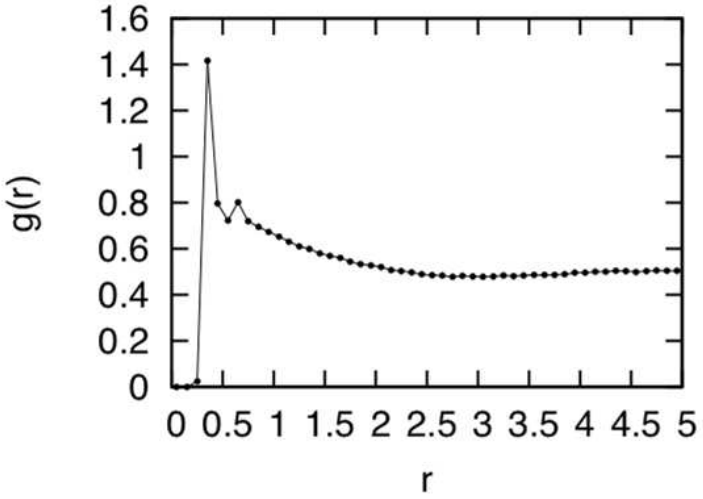

Figure 23: The pair distribution function corresponding to the simulation of figure 22. Note the peak at approximately 0.3 which is the boat diameter.

3.5 Other observations: intermittent motion and long term memory

Intermittent motion has been observed in experiment [31, 29] and reproduced in simulation by introducing a nonconstant diffusion rate as described in section 2.3.3. Such motion can also be demonstrated using the basic model with constant diffusion rate by making the diameter of the plastic disk much larger than the camphor disk and using a very slow diffusion rate of about $0.01cm^2/s$. Figure 24 shows four interesting intermittent behaviors. In figure 24.a, the boat periodically moves and stops with a very regular period. The motion is always in the same direction even though the boat is symmetric. The motion in figure 24.b is similar, but the boat briefly moves in reverse before coming to rest and occasionally switches direction for one or more periods. The important difference between these two simulations is the size of the plastic disk. In 24.a the disk has a diameter of $1cm$ while in 24.b it is $1.5cm$ and both have a camphor diameter of $0.3cm$. Decreasing the diameter of the plastic disk further causes the intermittent behavior to stop and the boat to move at constant speed. When several boats are placed in a simulation corresponding to 24.b, the period is somewhat irregular and the boats often change direction due to collisions and a more complicated camphor field. This is shown in figure 24.c.

Finally, figure 24.d shows a long term memory effect caused by using such a slow diffusion rate. In this case the plastic disk is the same size as the camphor disk. The camphor density in the region where the boat stops increases significantly compared to the areas in which it moves quickly. Since the diffusion rate is so slow, this peak remains for a long time. Each time the boat approaches the peak it slows down and eventually stops, reinforcing the peak with additional camphor. Such long term memory is also seen in some experiments, but a sufficient correspondence between experiment and simulation has not yet been demonstrated.

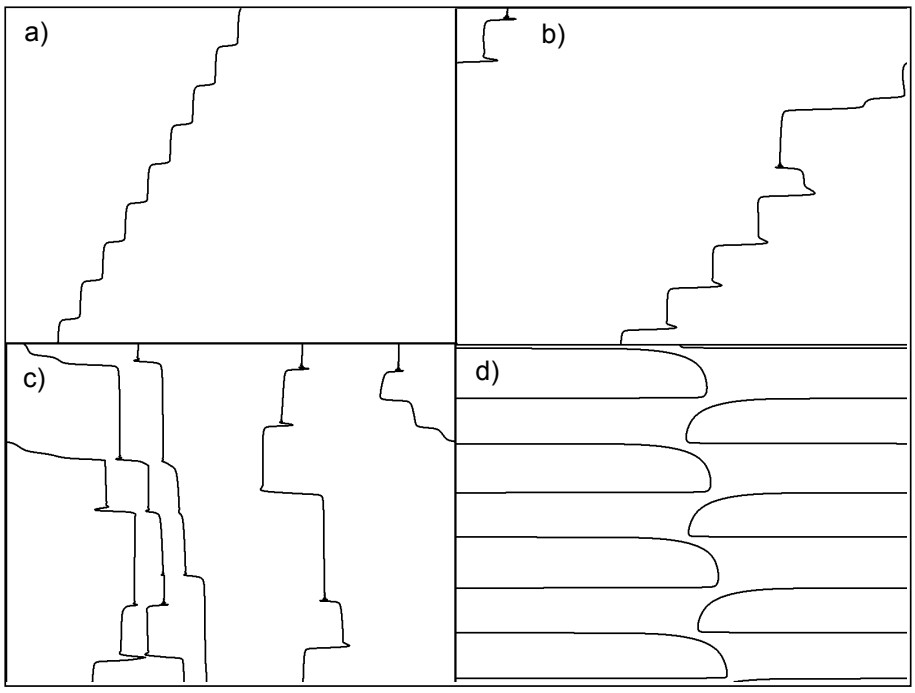

Figure 24: Intermittent motion of a boat with *a)*$1cm$ and *b)*$1.5cm$ plastic disk diameter. *c)*Five boats with $1.5cm$ plastic disks. *d)*Long term memory effect caused by very slow diffusion rate.

Appendices

A Constant velocity solution for one boat

The camphor field created by one boat moving at constant velocity is described by the traveling pulse equation.

$$-v\nabla c = \Delta c - kc + \alpha F(x - x_0) \tag{17}$$

The following solution is adapted from Nagayama *et al.* [20] It assumes that the route length is sufficiently long that the profile of c is well localized. This allows us to adopt the boundary condition $\lim_{|x|\to\infty} c(x) = 0$ and continuity condition, $c(x) \in C^1(\Re)$. Also, we will use the slightly different dimensionless parameters $c = \frac{c}{\alpha}$ and $\beta = \beta\alpha$ to simplify the calculation. The solution is

$$c(x) = \begin{cases} A_1 \exp\left(\frac{1}{2}\eta_+ x\right) & x < -r_0 \\ A_2 \exp\left(\frac{1}{2}\eta_+ x\right) + B_2 \exp\left(\frac{1}{2}\eta_- x\right) - \frac{1}{k} & -r_0 < x < r_0 \\ B_3 \exp\left(\frac{1}{2}\eta_- x\right) & x > r_0 \end{cases} \tag{18}$$

where

$$\begin{aligned} A_1 &= \tfrac{\eta_-}{2k\eta}\left(\exp\left(-\tfrac{\eta_+}{2}r_0\right) - \exp\left(\tfrac{\eta_+}{2}r_0\right)\right) \\ A_2 &= \tfrac{\eta_-}{2k\eta}\exp\left(-\tfrac{\eta_+}{2}r_0\right) \\ B_2 &= -\tfrac{\eta_+}{2k\eta}\exp\left(\tfrac{\eta_-}{2}r_0\right) \\ B_3 &= \tfrac{\eta_+}{2k\eta}\left(\exp\left(-\tfrac{\eta_-}{2}r_0\right) - \exp\left(\tfrac{\eta_-}{2}r_0\right)\right) \\ \eta &= \sqrt{v^2 + 4k} \\ \eta_\pm &= -v \pm \eta \end{aligned} \tag{19}$$

The values of this solution at the two edges of the boat, $x = \pm\frac{L}{2} = \pm 2r_0$ are then

$$\begin{aligned} c_+ &= c(2r_0) = B_3 \exp\left(\eta_- r_0\right) \\ c_- &= c(-2r_0) = A_1 \exp\left(-\eta_+ r_0\right) \end{aligned} \tag{20}$$

Substituting these and the constant velocity, v, into the equation of motion gives

$$0 = -\mu v + \Gamma\left[\frac{1}{\beta B_3^2 \exp\left(2\eta_- r_0\right) + 1} - \frac{1}{\beta A_1^2 \exp\left(-2\eta_+ r_0\right) + 1}\right] \tag{21}$$

Note that if $v = 0$, $A_1 = B_3$ and $\eta_+ = -\eta_-$, so the equation of motion is satisfied for any value of μ. We can also rearrange the equation to give viscosity as a function of equilibrium velocity.

$$\mu(v) = \frac{\Gamma}{v}\left[\frac{1}{\beta B_3^2 \exp\left(2\eta_- r_0\right) + 1} - \frac{1}{\beta A_1^2 \exp\left(-2\eta_+ r_0\right) + 1}\right] \tag{22}$$

This was used to produce the analytical solutions shown in figure 18. Inverting this relationship results in a bifurcation as shown in the figure. By changing β in this equation, the bifurcation changes between subcritical and supercritical. Recalling the different dimensionless parameters used here, this is equivalent to changing α for the parameters used in the main part of the text.

B Additional spatio-temporal diagrams

Here are several figures displaying the different types of oscillatory behavior observed for different viscosities.

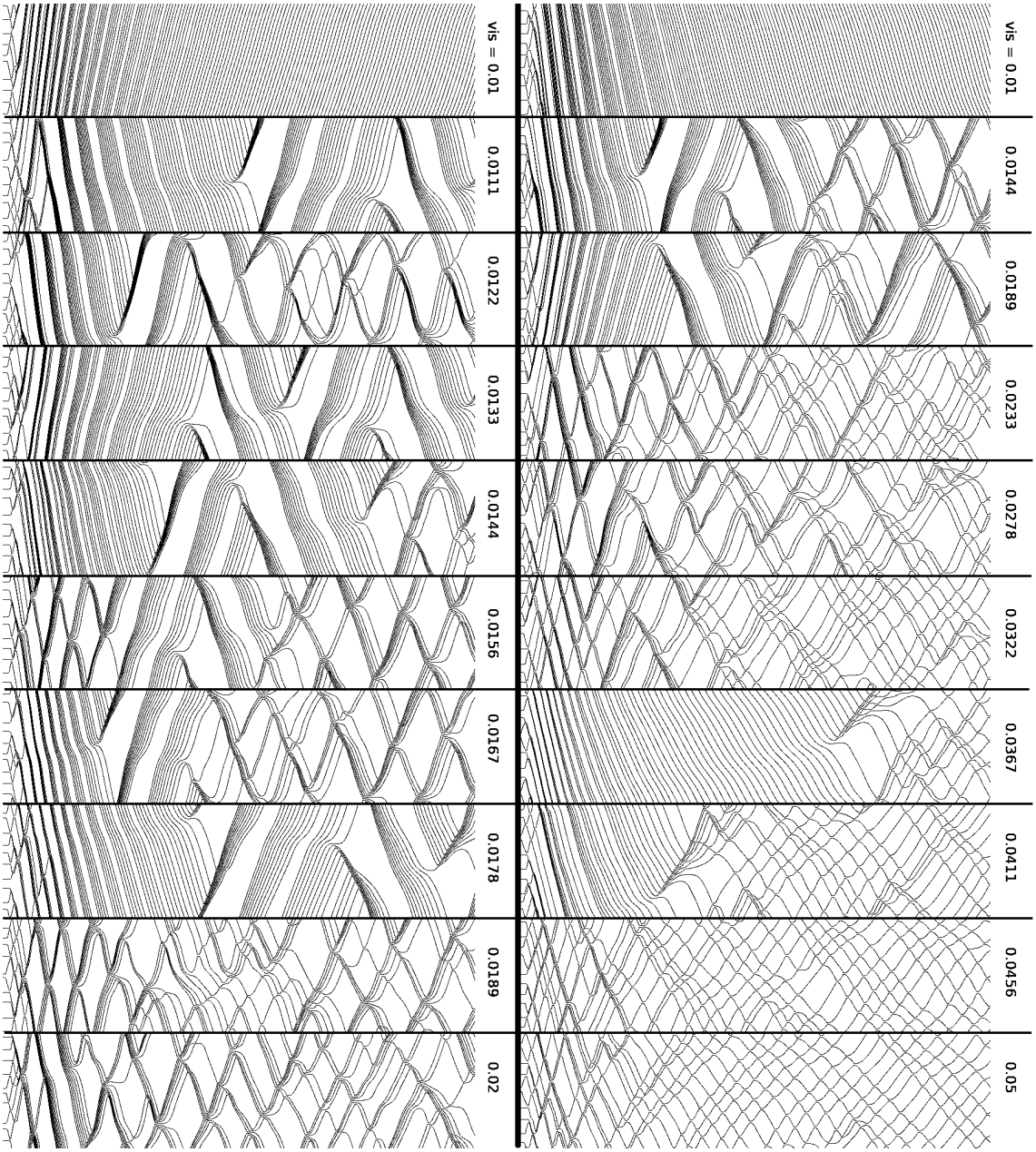

Figure 25: (Figure rotated clockwise) Spatio-temporal diagrams for the labeled viscosities with $N = 10$. The right(upper) diagrams are for μ =0.01 to 0.05. The left(lower) diagrams are a more detailed look at μ =0.01 to 0.02.

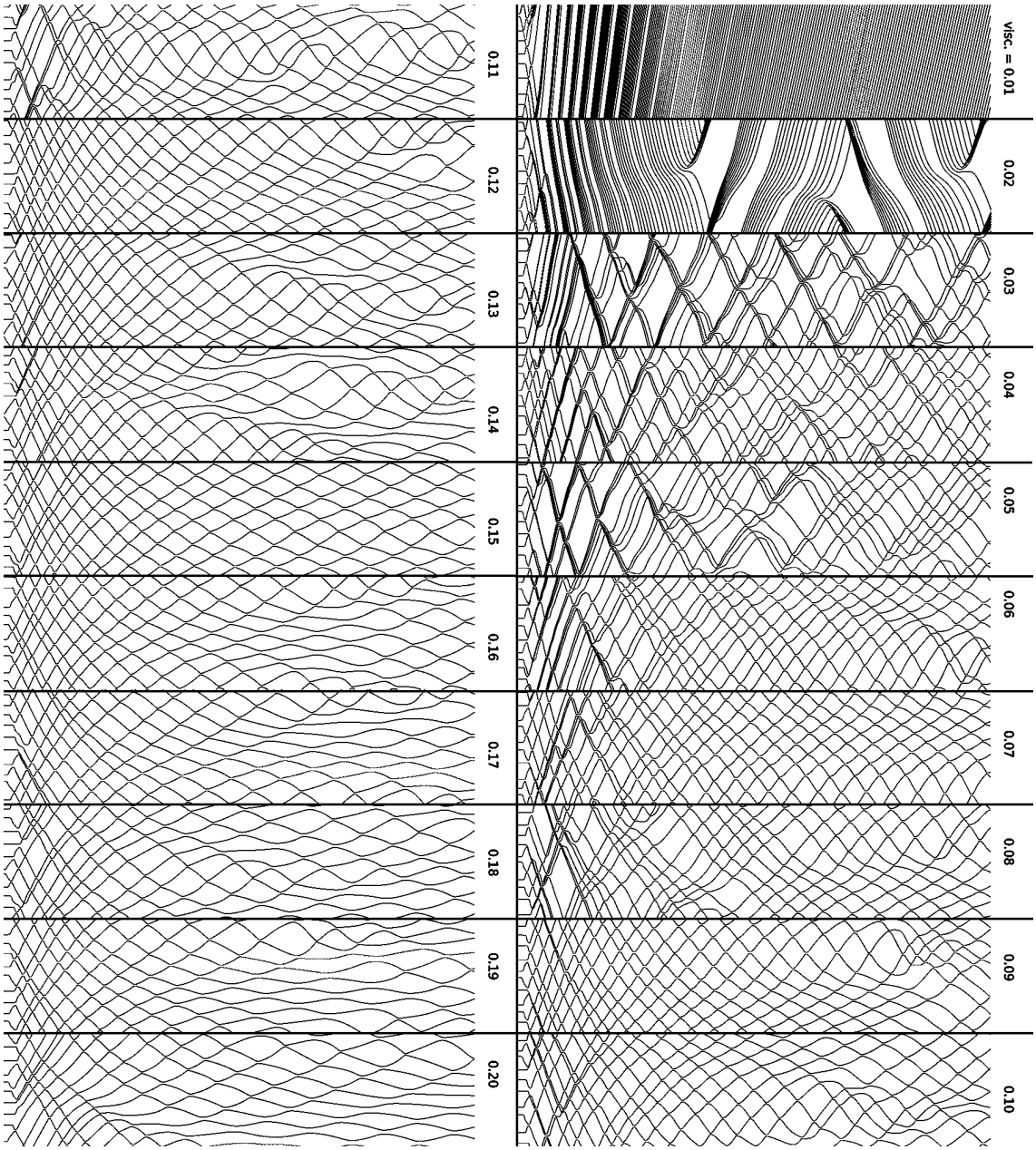

Figure 26: (Figure rotated clockwise) Spatio-temporal diagrams for the labeled viscosities with $N = 10$. Here, μ =0.01 to 0.02.

References

[1] S. Nakata, Y. Doi, and H. Kitahata: J. Phys. Chem. B **109** (2005) 1798.

[2] D. L. Blair, T. Neicu, and A. Kudrolli: Phys. Rev. E **67** (2003) 031303.

[3] J. Deseigne, O. Dauchot, and H. Chaté: Phys. Rev. Lett. **105** (2010) 098001.

[4] N. J. Suematsu, S. Nakata, A. Awazu, and H. Nishimori: Phys. Rev. E **81** (2010) 056210.

[5] E. Heisler, N. J. Suematsu, A. Awazu, and H. Nishimori: Phys. Rev. E **85** (2012) 055201.

[6] E. Heisler, N. J. Suematsu, A. Awazu, and H. Nishimori: J. Phys. Soc. Japan **81** (2012) 074605.

[7] T. Vicsek, A. Czirók, E. Ben-Jacob, I. Cohen, and O. Shochet: Phys. Rev. Lett. **75** (1995) 1226.

[8] A. Czirók, A.-L. Barabási, and T. Vicsek: Phys. Rev. Lett. **82** (1999) 209.

[9] H. Levine, W.-J. Rappel, and I. Cohen: Phys. Rev. E **63** (2000) 017101.

[10] G. Grégoire and H. Chaté: Phys. Rev. Lett. **92** (2004) 025702.

[11] A. Czirók, H. E. Stanley, and T. Vicsek: J. Phys. A: Mathematical and General **30** (1997) 1375.

[12] E. Bertin, M. Droz, and G. Grégoire: Phys. Rev. E **74** (2006) 022101.

[13] M. R. D'Orsogna, Y. L. Chuang, A. L. Bertozzi, and L. S. Chayes: Phys. Rev. Lett. **96** (2006) 104302.

[14] A. Baskaran and M. C. Marchetti: Phys. Rev. Lett. **101** (2008) 268101.

[15] S. Mishra, A. Baskaran, and M. C. Marchetti: Phys. Rev. E **81** (2010) 061916.

[16] S. Nakata, Y. Iguchi, S. Ose, M. Kuboyama, T. Ishii, and K. Yoshikawa: Langmuir **13** (1997) 4454.

[17] S. Soh, M. Branicki, and B. A. Grzybowski: J. Phys. Chem. Letters **2** (2011) 770.

[18] Y. Hayashima, M. Nagayama, and S. Nakata: J. Phys. Chem. B **105** (2001) 5353.

[19] S. Nakata, Y. Hayashima, and T. Ishii: Colloids and Surfaces A: Physicochemical and Engineering Aspects **182** (2001) 231 .

[20] M. Nagayama, S. Nakata, Y. Doi, and Y. Hayashima: Physica D: Nonlinear Phenomena **194** (2004) 151 .

[21] H. Kitahata, S.-i. Hiromatsu, Y. Doi, S. Nakata, and M. Rafiqul Islam: Phys. Chem. Chem. Phys. **6** (2004) 2409.

[22] Y. Hayashima, M. Nagayama, Y. Doi, S. Nakata, M. Kimura, and M. Iida: Phys. Chem. Chem. Phys. **4** (2002) 1386.

[23] S. Nakata and K. Matsuo: Langmuir **21** (2005) 982.

[24] S. Nakata and J. Kirisaka: J. Phys. Chem. B **110** (2006) 1856.

[25] S. Nakata, J. Kirisaka, Y. Arima, and T. Ishii: J. Phys. Chem. B **110** (2006) 21131.

[26] O. Schulz and M. Markus: J. Phys. Chem. B **111** (2007) 8175.

[27] S. Soh, K. J. M. Bishop, and B. A. Grzybowski: J. Phys. Chem. B **112** (2008) 10848.

[28] M. I. Kohira, Y. Hayashima, M. Nagayama, and S. Nakata: Langmuir **17** (2001) 7124.

[29] N. J. Suematsu, Y. Ikura, M. Nagayama, H. Kitahata, N. Kawagishi, M. Murakami, and S. Nakata: J. Phys. Chem. C **114** (2010) 9876.

[30] A. John, A. Schadschneider, D. Chowdhury, and K. Nishinari: Phys. Rev. Lett. **102** (2009) 108001.

[31] S. Nakata, Y. Doi, and Y. Hayashima: J. Phys. Chem. B **106** (2002) 11681.